Applied Energy 376 (2024) 124293

Contents lists available at ScienceDirect

Applied Energy

journal homepage: www.elsevier.com/locate/apenergy

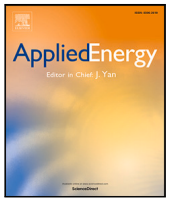

Experimental assessment of a heavy-duty fuel cell system in relevant operating conditions

Jose M. Desantes, R. Novella, M. Lopez-Juarez *, I. Nidaguila

CMT - Clean Mobility & Thermofluids, Universitat Politècnica de València, Camino de vera s/n, 46022 Valencia, Spain

ARTICLE INFO

Keywords:
Hydrogen
Proton exchange membrane fuel cell system
Experimental characterization
Steady-state
Heavy-duty vehicle application
Polarization curve sensitivity

ABSTRACT

During the past few years, the research interest in fuel cell systems (FCS) has increased significantly. Thus, this kind of powertrain is now at high Technology Readiness Levels (TRLs) and even starting to be commercialized. However, the currently available technology still has room for optimization. The existing bibliography shows studies mainly related to stack-level characterization or FCS studies with a poor level of detail. The present paper focuses on producing a detailed database about the performance of a specific FCS designed for heavy-duty vehicle (HDV) applications. The obtained dataset provides information about the influence of ambient conditions on the performance of the system, plus information about the anode and cathode circuits. These factors represent an important novelty with respect to other pieces of literature present in the actual research framework. Additionally, the obtained data regarding the performance of an FCS is highly significant for HDV manufacturers in the transportation sector and eases the pathway to the optimization of these technologies. The written piece of research proves the importance of studying the ambient conditions. The experimental campaign has shown that increasing relative humidity can improve the performance of the membrane up to a 2% for a 25% change in the humidity level. Additionally, the study shows the importance of implementing an appropriate supply gas strategy, both for anode and cathode, and designing the right purging mechanisms for H_2 at the anode inlet. The obtained results show how there exist a relation between the optimal efficiency operating point and a H_2 excess from the supply strategy.

1. Introduction

At present times, there exists a high awareness about the global environmental crisis. During the last few years, the temperature of the earth has increased ~1 °C and this temperature difference is expected to reach 1.5 °C if the increasing rate does not change [1]. This global warming emergency is the main reason why the interest in decarbonization has risen recently [2]. In this context, hydrogen (H_2) has proved to be a versatile energy carrier that can be produced from different existing energy sources (steam methane reforming or *SMR*, electrolysis by using electricity or renewable energies...). Additionally, it can be converted to energy for a wide variety of applications. The use of H_2 as fuel will ease the path to limiting the global temperature increase to 2 °C [3] and the reduction of greenhouse gases (GHG) emissions due to the low-carbon footprint of its use [4]. This energy vector will primarily be used in the transportation sector as fuel for FCS [5] or Internal Combustion Engine (ICE) [6]. One of the main challenges of the use of H_2 as a fuel comes from its production-associated emissions [7]. However, it has been proved through Life Cycle Assessment (LCA) studies that there are several production pathways that could lead to low emission scenarios [8].

The importance of decarbonizing the transportation sector comes from its high contribution in the current global emissions. In 2022, the transport industry produced around 8.1 billion tonnes of equivalent CO_2 [9], which represents a 20.7% of the total global GHG emissions. Thus, it is the second most polluting industrial sector [10]. From this data, it is interesting to note that road transport represents a 79% of these emissions, from which a 31% comes from HDV applications [11]. Thus, reducing the emissions in this particular sector would be highly beneficial in the path to decarbonization. In this context, FCS provide a reliable decarbonization strategy for these kinds of vehicles. Nowadays, most heavy-duty (HD) manufacturers (Hyundai, IVECO, VOLVO, etc.) are looking into the FCS propulsive system to include it in their trucks [12]. However, the majority of the current heavy-duty fuel cell vehicle (HDFCV) are still in the development stage, thereby opening the way for an in-depth study of the subject.

As the research into these technologies has increased during the past decade, researchers are starting to look into different matters aside from

* Corresponding author.
E-mail address: marlojua@mot.upv.es (M. Lopez-Juarez).

https://doi.org/10.1016/j.apenergy.2024.124293
Received 22 May 2024; Received in revised form 11 July 2024; Accepted 16 August 2024
Available online 22 August 2024

its technical development. The deployment of this kind of powertrains would require a mass investment and new infrastructure. The economic matter is highly significant in the viability of any new technology, thus, many authors have done techno-economic analyses [13] that shed some light into this issue. Furthermore, most of these studies focus on the specific cost of the green H_2 development, as in [14]. The insights provided by TEA tools are indispensable for stakeholders across the H_2 value chain, from researchers and engineers to policymakers and industry leaders, as they work towards a sustainable and economically viable future. As HDVs are one of the key markets in which FCS are expected to be used mostly, TEAs have already analyzing this specific sector, as done in [15].

As part of the road vehicle sector and, particularly, freight transportation, it may seem that HDVs are comparable to Light Commercial vehicles (LCVs). However, the needs of these commercial vehicles are very different. Firstly, there exists a wide variety of road freight transport vehicles depending on the weight they are able to carry. LCVs are capable of carrying woods with a total weight not higher than 3.5 tonnes. However, medium duty (MD) trucks can carry from 3.5 up to 12 tonnes and HD trucks over 12 tonnes [16]. The total weight of the vehicle is an essential factor in the choice of its propulsive system, but also it has an important influence on its driving conditions. HDV are usually driven along predefined routes or standard driving profiles if they are used for off-road applications. These kind of driving conditions are mainly steady-state (HHDDT or Heavy Heavy-Duty Diesel Truck), which means the truck in which the FCS will be used, will mainly be driven at constant speed. This constant speed allows the FCS to work under steady and high efficiency conditions. Nevertheless, LDVs are designed to be used under a more unpredictable set of driving conditions. As this kind of vehicles are mainly used in urban environments, they require a FCS which is designed to be used dynamically (Worldwide Harmonized Light Vehicles Test Cycle or WLTC cycles).

The present research framework shows an increasing interest in using FCS for HDVs. Several HD truck manufacturers as Hyundai (Hyundai XCIENT), Nikola (Nikola Tre FCEV) and Hyzon (Hyzon HyMax Series) are starting to commercialize their FCS solutions for long-haul freight transportation. However, there are still several issues related to H_2 technologies that need to be solved (H_2 delivery, refueling, production...), as there needs to be a global investment to make this energy source become a reality. Additionally, these kind of vehicles are still in low TRLs, which means their manufacturing process, and therefore its cost, is high. There exists several ways to reduce costs in this phase (research investment, mass production of the technology...). However, when thinking about the performance of the vehicle, there is still work to be done until its optimal efficiency is reached. Thus, a deep analysis into the performance of a real FCS and its later analysis would provide highly significant data in the present research framework.

The increasing interest in HDFCV led to the study of these systems using simulating tools, as in [17]. The existing studies usually focus on the architecture of the powertrain [18] or the control strategy of the system [19]. Nonetheless, as FCS become a reality, it is important to improve the existing models with real data from experimental testing activities [20].

When performing an exhaustive bibliographic research work, it is easy to note that most experimental papers study single proton exchange membrane fuel cell (PEMFC) as in [21] or small stacks as seen in [22]. The existing analysis of the single cell mainly focuses on optimizing the electrochemical reaction by improving the different layers that compose the FC, as in [23,24]. Reviewing the available stack-related studies closely reveals that they cover a wide range of subjects. In [25], Tang et al. analyze the heterogeneity in the stack performance by comparing the different cells. Other authors, as Hoa et al. in [26], study specific procedures as start-up and shutdown, the cold start process [27], lifetime of the cell [28] or characterize the performance of the stack [29]. Despite the high amount of stack studies, it is hard to find experimental works that analyze the performance of the stack together with its integrated Balance of Plant (BoP). In [30], Zhang et al. assemble a BoP to simulate the testing and characterization of a complete FCS. This study is quite interesting and provides significant data for FCS manufacturers. Nonetheless, as with other of the existing bibliographic sources, it lacks information about how a complete and integrated system would work. The mentioned bibliographic sources present data of high research interest, but the integration of a FCS into a vehicle requires the understanding of the complete system, in which the stack works together with its BoP elements. Nevertheless, as it has been previously shown by means of several high interest research works, the existing literature focuses on cell and FC stack studies rather than FCS.

The integration of a complete FCS into a vehicle requires a complex system to correctly fit the inlet and outlet requirements of the FCS. The way in which the fluids go into the system may influence its efficiency. The currently available research works which focus on the anode of H_2 circuit mainly study different kind of flow fields into cells, as shown in [31,32]. However, these kind of studies focus on the distribution of the fluid along the membrane and its effects on the electrochemical reaction rather than the amount of fluid going in and out of the system. Other studies such as [33] study the H_2 inlet into a single cell and its relation to water management and cell functioning. This study provides relevant data to the literature, but it does not study the H_2 purge or the effect on a complete system rather than a single cell.

On the cathode circuit side, there exist research paper that look into different geometries of the flow field to improve the electrochemical reaction [34], as seen with the anode circuit. Additionally, some existing works also research about the use of different materials in the cell [35]. As these papers provide valuable information to the current bibliographic framework, it still lacks information about the complete cathode system. The use of a FCS in a vehicle requires the conditioning of the air flow by using a compressor and its performance is not trivial in the efficiency of the system and the conditions the air mass flow goes through.

Unfortunately, for now, there exist no available datasets for real complete FCS with their BoP in the literature. Thus, researchers have little real information about the previously stated matters.

As a consequence, to fill this knowledge gap, in previous papers, the authors of the present paper studied the performance of the whole FCS integrated in a vehicle, but following a 0D–1D modeling approach [36] and even developing an own simulating tool for FCS [37]. As there was no possibility to acquire real data, the authors elaborated simulation models to approach the study of FCVs in the best known possible way for that moment.

Furthermore, other authors have been looking into the use of FCS for the HDV sector. As previously explained, the low TRLs in which this powertrains are at the moment leads to studies and analyses which are mainly based on modeling activities. Most of the authors focus their research work into the study of different energy management strategies (EMS) to control the hybrid vehicles as [17,38]. However, other essential issues regarding FCHDVs as emissions [39] or durability [40] are also being studied.

Additionally, a HDFCV would work under very different ambient conditions depending on its working area. Thus, it would be highly significant to understand how different air inlet conditions influence its performance. Yang et al. study these effects by using simulating tools [41], but producing empirical data about this would represent an important novelty in the field, as there are no currently available datasets regarding the real performance of a FCS under different operating conditions. As it has previously been remarked, the study of a stack together with its BoP would provide significant data about the performance of the anode and cathode circuit, as well as the efficiency of the complete system. Understanding the performance of the FCS rather than the stack is highly significant as this is the system which will later be integrated into a real vehicle.

1.1. Knowledge gaps

Considering the available data and studies in the literature explained in Section 1, the present study looks into some of the existing knowledge gaps in the fuel cell sector. These knowledge gaps can be summarized as follows:

1. There exist a limited number of experimental research works that analyze the influence of operating conditions, such as temperature (T) and relative humidity (RH) of air, on the performance of a complete FCS designed for HD applications. Most existing studies on FCS performance do not include a dedicated analysis of ambient conditions. Additionally, the studies that do examine the influence of air temperature and humidity typically focus on cell or stack performance and do not provide comprehensive BoP data. Furthermore, there are currently very few papers that include data on real HD FCS.
2. The existing data about the anode circuit in the literature focuses on the mass flow into the stack rather than giving information about the complete anode circuit. Most existing studies on PEMFC systems focus primarily on the electrochemical process on the membrane and how to improve it. Specific details about the supply gas systems in the anode and cathode are rarely studied in depth or shared. Understanding the H_2 mass flow entering the system, the purging strategy, and the amount of gas consumed would provide valuable insights for optimizing these technologies.
3. As the existing literature focuses on cell and stack data, there exists limited information about the complete cathode circuit. Understanding the relationship between the BoP power, the cathode inlet mass flow, and stoichiometry is crucial for improving the efficiency of the FCS.
4. Absence of an FCS database for the specific use in HD trucks in the literature. Currently, the available experimentally based FCS models are mainly validated with data from FC or FC stack. Furthermore, the existing experimental campaigns that include FCS are designed to be general and be used for different kind of vehicles. However, as the HD sector is one of the most probable uses of PEMFC, it would be highly significant to generate a database with data from a HD designed FCS to feed a driving simulation model for a virtual truck.

From the previous considerations, it is evident how the effect of operating conditions on a FCS represents an unexplored field of interest in the current FCS market. In addition, having a more clear representation of the work of the anode and cathode circuits could be significant in the improvement of these powertrains. Finally, all these previously stated data could have a great importance in the generation of a FCS database for future simulation models that would allow the optimization of FCS propulsive systems.

1.2. Contribution and objectives

The main objective of this paper consists of obtaining insight into how a state-of-the-art FCS works under steady-state conditions and obtaining a set of data representative of its performance that can be used to improve the existing models. The final objective of the paper is to cover the knowledge gaps regarding the existing FCS studies present in the literature (Section 1.1). The specific contributions to achieving such an objective are:

- Analyze the effect of the ambient operating conditions, both temperature and relative humidity, on the steady-state performance of the FCS (knowledge gap 1).
- Study in detail the performance of the anode circuit. Understand the specific H_2 supply and purging strategy of the FCS (knowledge gap 2).
- Understand the evolution of the cathode stoichiometry in a real FCS and how the operating conditions influence it (knowledge gap 3).
- Obtain a global understanding of the steady-state performance of an FCS and have a dataset that would allow the validation of numerical models (knowledge gap 4).

The accomplishment of the previously stated tasks would lead to the achievement of the final goal of this study and filling the current knowledge gaps in the field (Section 1.1).

Table 1
Tested FCS technical specifications.

FCS specifications	Value
Max. power [kW]	60
Max. stack current [A]	350
Min. stack current [A]	62.5
H_2 inlet [bar]	12.5–15
Air inlet [bar]	0.7–1.05

2. Methodology

The present study requires a complex experimental facility and a specific set of procedures that need to be followed. The performed testing campaign analyses the performance of an FCS, which considers the FC and its BoP. The main amount of experimental FC-based papers that can be found in the literature considers only the testing of the stack in less detailed testbenches. Thus, the use of a whole FCS represents an important advantage concerning the existing research and this whole set of components should be explained in detail (Section 2.1).

In addition, the study of the performance of an FCS is not trivial and it requires specific equipment. Each FCS has its particularities, therefore, for the correct of operation of the used FCS, some considerations have been made and certain devices have been included in the facility to ensure its correct operation (Section 2.2). The whole testbench in which the FCS with its BoP and the facility auxiliary equipment are shown is represented in Fig. 1.

Finally, the experimental campaign has been accomplished by strictly following the designed procedures (Section 2.3). This test set includes the specific steady-state experiments, but also certain procedures to ease the correct operation of the FCS (start-up and shutdown or *SUSD*, warm-up, emergency stops...).

2.1. Fuel cell system

The tested FCS includes an FC stack, its BoP, and an embedded controller. This engine has been designed to be included in a commercial vehicle, mainly for HD vehicles and is compatible with driving conditions. The present system is appropriate for its use in HDVs as it has been designed to work mainly under the typical low dynamic conditions that these vehicles usually work under. Steady and low dynamic conditions allow the maximum durability of this specific system. This information has been acquired from the FCS manufacturer.

This FCS can reach up to 60 kW of power and its product specifications are summarized in Table 1. It is important to remark that, due to confidentiality policies, there is information about the FCS that cannot be disclosed.

The reason behind the choice of this specific system comes from the fact that this FCS has been designed for HD use. The existing literature shows the importance of FCS in the freight transportation sector (Section 1), thus, being able to characterize the performance of a real HD FCS would be highly significant for this research line. The 60 kW power limit may seem low for an HDFCV, but this is a response to the current modular trend in the design of these vehicles. At present times, the use of a modular powertrain is a key research topic [18] and most manufacturers have already chosen this solution

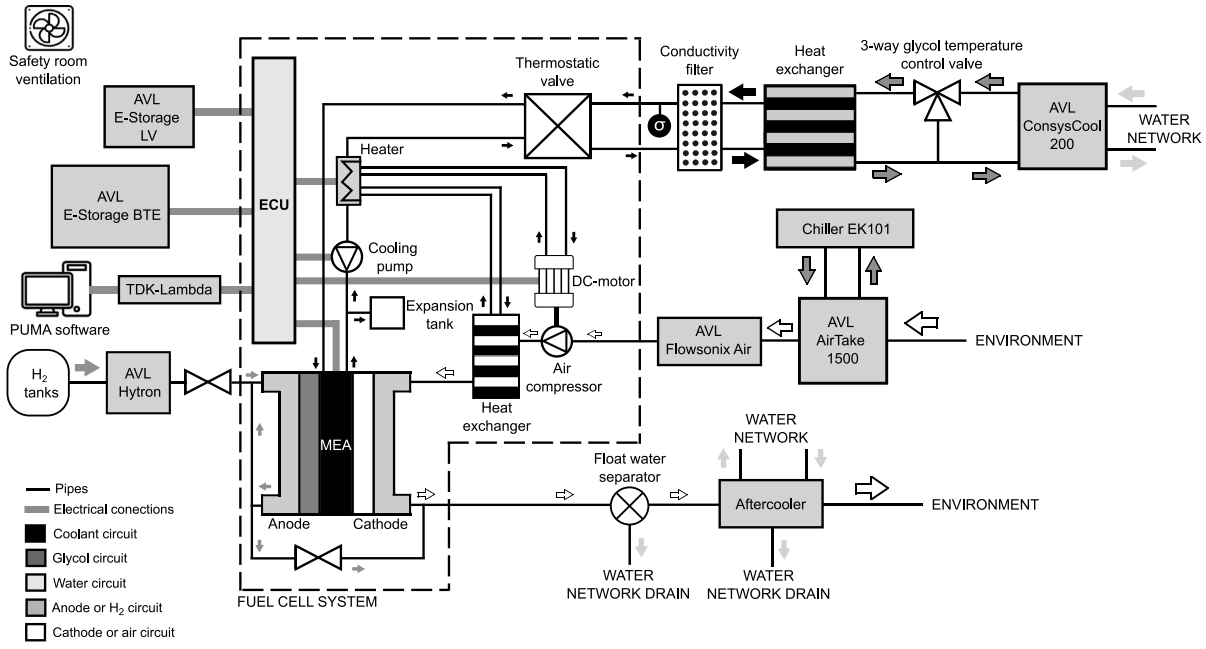

Fig. 1. FCS and testbed scheme.

for their vehicles or prototypes. In [12], it can be noted that in the current HDFCV scenario, there exist several modular FC trucks with a wide variety of FC powers and sizes, from 30 kW to 150 kW. Thus, a 60 kW FCS represents a good value for an HDFCV.

In addition, the present FCS would also be a good choice for the LCV market. This vehicle sector has been less studied for now, but some manufacturers have already presented their prototypes. The architecture of the powertrain for this kind of commercial vehicle has not been defined yet [42], but some manufacturers have presented a hybrid vehicle with a medium-size FCS. Stellantis proposes a hybrid LCV that uses a medium-sized FCS [43] similar to the studied one. In conclusion, the studied FCS can be considered a good representation of the market FCS for on-road vehicles.

2.1.1. Balance of plant

The studied propulsive system includes the FC stack and a set of components to condition the fluids that go into the stack and control and monitor the electrical signals used. The system is mainly composed of 4 different circuits: anode, cathode, cooling, and electrical.

The anode or H_2 circuit is composed of the main flow that goes into the stack and a secondary inlet that comes from the anode outlet and is recirculated into the stack. Thus, the anode outlet is connected both to the inlet and an exhaust pipe.

The cathode or air circuit is more complex. The air comes into the system at ambient pressure and goes through a air compressor, which is powered by an e-motor. Then, the air that flows out of the compressor passes through a heat exchanger that decreases its temperature to go into the stack at an appropriate temperature. Finally, the cathode outlet is connected to the anode outlet that takes the exhaust gases out of the system. For the correct performance of all this equipment, a cooling circuit interacts with the elements of the BoP to ensure safe temperature operations. This system is composed of a set of pipelines in which low-electrical-conductivity coolant at low temperatures flows along the system. The temperature of the BoP components is controlled by a thermostatic valve which lets the right amount of coolant into the system. This fluid passes through the FC stack to cool it down due to the heat release in the electrochemical process. However, it is also used to control the temperature of the e-motor and the temperature of the air going into the Finally, the FCS is controlled by an ECU. This control unit demands the required power or current to the stack and, consequently, monitors the cooling pump, heater, and DC motor to produce the appropriate conditions in the performance of the system to meet the current specifications.

Table 2
AirTake 1500 technical specifications [44].

AT 1500 specifications	Value
Air flow outlet [m^3/h]	1500
Min. outlet T [°C]	15
Max. outlet T [°C]	40
T accuracy [°C]	±1
Min. outlet RH [%]	20
Max. outlet RH [%]	80
RH accuracy [%]	±5

2.2. Testing facility

The testing facility used is composed of a set of different devices that allow the system to work correctly and record and store the desired data results. As shown in Fig. 1, the testbench can be divided into two main parts: the electrical circuit and the flow pipes. In addition, it is important to remark that there is a main part of the testbench that would be common to any FCS testing. However, some of the equipment has been included for the specific tested powertrain.

2.2.1. FCS testing equipment

The testing facility devices that are common for any FCS include the air, H_2 and coolant inlets, as well as the electrical supplies and control units.

The air that flows into the cathode comes from the ambient. However, the experimental setup can change the air conditions by using the AVL List GmbH (AVL) AirTake 1500. This system regulates the temperature and humidity of airflow according to the technical specifications shown in Table 2.

The conditioning system is mainly composed by a fan, two heating coils, a cooling system, and a humidifier. The minimum temperature reached by the AirTake 1500 depends on the glycol circuit of the device. In this case, the cold supply that flows into the system is provided by the EK101 chiller, which allows it to reach temperatures up to 13 °C in the fluid.

Table 3
H_2 generation facility.

Generated H_2 specifications	Value
Purity [%]	99.999
Production [kg/h]	0.71
Storage pressure [bar]	330
Storage capacity [kg]	130

Table 4
AVL Hytron technical specifications.

Hytron specifications	Value
Inlet limits [bar]	4 to 30
Outlet limit [bar]	20
H_2 supply accuracy [%]	±1

Table 5
AVL ConsysCool 200 technical specifications.

ConsysCool 200 specifications	Value
Primary circuit operating range [°C]	5 to 85
Secondary circuit operating range [°C]	20 to 140

After the conditioning process inside the AirTake 1500, the air goes through a set of particle filters that ensure the airflow is at the proper conditions when going inside the FCS.

The conditioned mass flow of air goes into the system by using the AVL Flowsonix Air [45]. This device is an air mass flow meter, which uses ultrasonic sensors to measure accurately the airflow going inside the cathode inlet.

The anode circuit is composed of the H_2 supply and the control of the inlet mass flow. The H_2 used for the present testing activities comes from a H_2 generation facility. To ensure the compatibility of the generation facility to any FCS, the H_2 produced has a high level of purity, as it can be seen in 3.

The stored H_2 at 330 bar goes through an expansion process that leaves this gas at 25 bar when it enters the FCS room facility. Then, the conditions of the inlet gas that goes into the anode circuit are controlled by the AVL Hytron (see Table 4). This device is a H_2 high-precision supply and consumption measurement system. The system also includes N_2 and compressed air used to purge the system and ensure the high purity of the gas going inside the FCS.

The high amount of heat released during the electrochemical reaction and the heat produced by the BoP elements of the system make the cooling circuit an unavoidable part of any FCS. The feed of coolant to the FCS requires a specific device capable of conditioning a fluid up to low-temperature levels. This facility uses the AVL ConsysCool 200 [46] for this purpose. This piece of equipment includes a water primary circuit and a glycol secondary circuit (Table 5). The secondary one goes into the testbed facility due to the low corrosive properties of this fluid and the water circuit is used to control the temperature of the glycol.

The testing of an FCS consists of the demand of different currents that simulate specific operating points or driving conditions representative of its performance when being integrated into a vehicle. Thus, a device capable of reproducing these conditions is required. The present testbed includes the AVL E-Storage BTE, which is a battery tester and emulator capable of generating power demands and supplies up to 250 kW. This power unit acts as the vehicle e-motor which would be connected to the FCS and is used to demand and receive the required current during the testing process.

In addition, the AVL E-Storage LV is also included in the testbed facility. This smaller power unit provides the required constant voltage (350 V) to the compressor. The other elements of the BoP require a lower voltage supply (27 V), which comes from the TDK-Lambda power unit.

The advantage of using this specific equipment provided by AVL is its easy integration and management. PUMA software allows to control of both the operation and data storage during the experimental activities.

2.2.2. Requirements for the owned FCS

The testing process of an FCS may have some particularities depending on the studied system. Thus, the testbed has been adapted to meet the requirements of the tested FCS, specifically, the cooling circuit needed some adjustments.

The used FCS includes its cooling circuit, which works independently with the cooling pump. Thus, there exists a flowing conflict with the pump of the ConsysCool 200. Therefore, a heat exchanger is used in the facility to control the temperature of the coolant circuit of the FCS without generating flux interferences. The temperature of the glycol coming from the ConsysCool 200 is managed by a 3-way valve controlled by a PID adjusted with the temperature requirements of the FCS.

The heat exchanged included in the experimental setup is a plate heat exchanger model S14A-ST. This system has a dissipation power of 114 kW for a temperature difference of 5 °C. Thus, it is over-dimensioned for the studied FCS, which usually presents a temperature gap of around 25 °C. However, this would allow the work with higher power FCS in future activities.

The coolant that needs to be used when operating an FCS has extremely low conductivity requirements. Thus, the cooling system of the FCS uses Glysantin FC G 20-00/50 to keep the temperature at an appropriate level. The advantage of glysantin concerning other glycol mixes is its long-term protection against conductivity increments. However, this fluid is quite corrosive and its conductivity is affected by the particles generated from flowing along the circuit.

Therefore, a continuous operation increases the conductivity, which could increase up to a dangerous level. A particle filter has been added to the system to restrict the coolant conductivity. The chosen filter is the Spectrapure MaxTemp DI_{TM} de-ionizing cartridge from SpectraPure, which can stand temperatures up to 80 °C.

Since the conductivity level is a significant parameter for the correct operation of the FCS, a high-quality conductivity sensor has been added to the circuit. The chosen sensor is the Burket Type 8222, which can measure between 0.05 μS/cm and 10 mS/cm. This precision allows for control of the conductivity level and keeps it around 1 μS/cm, which represents a safe value for the operation of the testbed.

Finally, in the cathode exhaust there exists a high production of water that can be reused by draining it into the water network. For this purpose, a float water separator is included right after the exhaust to remove the liquid water. After that, an aftercooler condensates the exhaust water vapor to the liquid phase so that it can easily be added to the building water network.

2.3. Experimental procedures

The experimental activities were performed following specific testing procedures reported in the literature. Before starting the testing campaign, the FCS provider carried out a commissioning process in which some start-up, shutdown, and safety procedures were included in the control software of the testbed.

The present study considers steady-state condition testing, which means the FCS should be as stable as possible. The performance of the stack is very sensitive to its temperature during the operation, which is between 50 and 70 °C. However, right after the start-up, the FC stack is still below its desired temperature. Thus, a warm-up routine (Fig. 2) has been designed to heat the stack to an appropriate temperature before starting the testing activities.

The warm-up process consists of a 4 step short test in which the current is increased slowly up to its maximum. The FCS is in idle conditions and it is immediately risen to 125 A. The first step is the

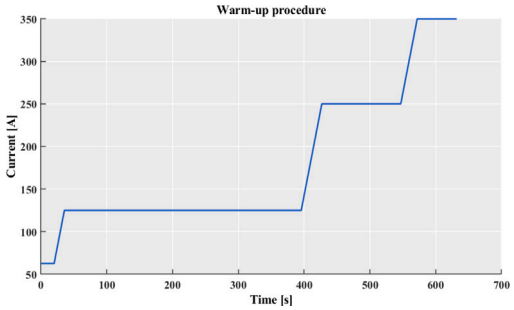

Fig. 2. Designed warm-up procedure to be performed after the start-up of the FCS.

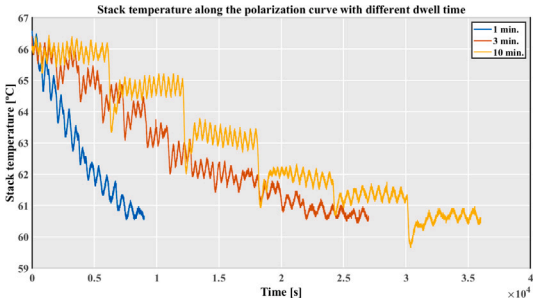

Fig. 3. Influence of the dwell time in the stack temperature stabilization along the polarization curve.

longest (6 min) and it has been empirically calibrated to allow the FCS to reach its proper stack temperature even when starting from cold ambient conditions. Then, the system current is increased to 250 A with a shorter waiting time and, finally, up to 350 A, in which the right stack temperature is rapidly reached.

The steady-state testing activities aim to understand the performance of the system and obtain a set of data useful to characterize it. Thus, the implemented testing procedure for this purpose is the polarization curve.

The polarization curve describes the performance of an FCS from the minimum to the maximum allowed current. It has three sections, each dominated by the reason of its voltage losses. However, due to confidentiality reasons, only the ohmic region of the polarization curve is analyzed in the present study.

The designed polarization curve test is based on the recommendations given by the Joint Research Center in [47]. It is a polarization curve that starts at maximum current, which allows good temperature control of the stack because of the previously explained warm-up process. In addition, the curve is defined by 15 points established by the % of maximum current [47].

The dwell time chosen for each point of the curve to emulate a steady-state performance is also chosen following the JRC procedure by considering 4 different periods: equilibration, stabilization, acquisition, and offset. The equilibration time considers the period in which the desired current is reached, stabilization time is the time considered until the performance of the stack is stable and the offset considers a small period before the next step. Then, the acquisition time is the period in which the measurement of the desired date is performed.

The JRC recommends a dwell time of 10 min for each step, but it states that this value depends on the testbed and the system used. Thus, the final user should establish this value considering the desired results and the characteristics of the experimental campaign. In this particular case, three different dwell times, of 1, 3, and 10 min, were tested before taking the final decision. The 1-min test showed that the measured parameters did not reach a stable value. The reason behind this was that the stack temperature was not able to settle to the appropriate value demanded by the ECU. The 10-min stabilization test was discarded due to its length in time. The proposed testing campaign required a large number of experiments, therefore, having a standard test feasible to be repeated several times without being excessively time-consuming, represents a significant issue. Finally, a dwell time of 3 min shows enough stabilization in the control variables, thus this is the chosen value. When considering the stabilization of the stack temperature, it is important to remark that this value is controlled by a PID that manages the coolant temperature. Thus, it is not possible to obtain a completely stable value. In this terms, a stabilization of this temperature means an oscillating value around a 0.7 °C deviation. This deviation is achieved both with the 3 min and 10 min dwell times.

Then, the test was designed considering the 4 time periods previously mentioned. The final time distribution and characteristics of the

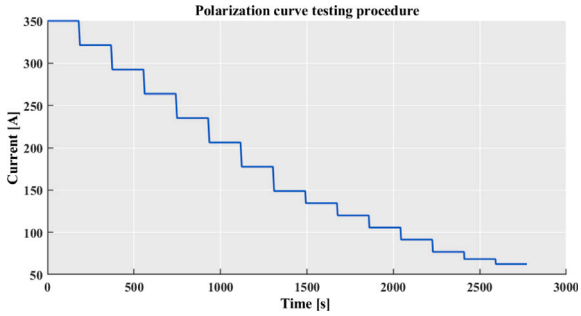

Fig. 4. Polarization curve testing protocol to be followed in the experimental campaign.

Table 6
Data used for the design of the polarization curve.

Test parameters	Values
Dwell time [s]	180
Dynamics, $I_t = \frac{dI}{dt}$ [A/s]	−4
Stabilization [s]	100
Acquisition [s]	60
Offset [s]	20

polarization curve are detailed in Table 6. The dynamics considered for the step change are a medium value that is not aggressive for the FCS.

Considering data in Table 6, the polarization curve that was reproduced under different conditions in this study is the one shown in Fig. 4.

Finally, before starting the experimental campaign, a validation process of the H_2 generation was performed. For this purpose, a rack of H_2 bottles of 99.999% purity was acquired and used in the testing facility. These tests were compared with the own produced H_2 under the same ambient and conductivity conditions to ensure there is no deviation in the produced results. The final results showed a power and voltage deviation lower than 0.7% and 0.6% respectively. Thus, the generated H_2 is considered appropriate for its use in the FCS.

3. Results and discussion

The data collected throughout the experimental campaign is thoroughly analyzed in this section. First of all, the performance of the FCS is described by studying in detail the obtained polarization curves. For this purpose, the results are analyzed independently to comprehend the effect of relative humidity and then, the effect of the ambient temperature.

After that, the performance of the anode circuit is studied to understand the H_2 supply and its relation with the efficiency of the system. Finally, the cathode circuit is also analyzed to get a global view of the functioning of the system.

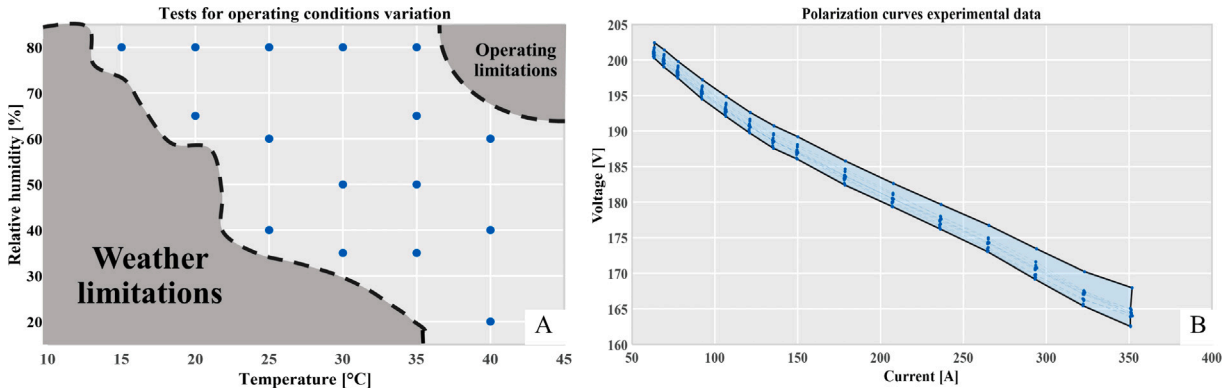

Fig. 5. (A) Temperature and relative humidity conditions in which the tests have been performed. (B) Polarization curves under the operating conditions in A.

3.1. Study of the polarization curve

The first part of the experimental campaign, explained in 2.3, focuses on understanding the effect of different ambient operating conditions on the performance of the FC stack. The polarization curve gives information about the FC performance by showing the relation between current and voltage. Thus, to understand how temperature and humidity affect the FC, the polarization curve for each different set of conditions is presented in Fig. 5.

Fig. 5A shows the ambient conditions in which polarization curve tests have been carried out. It is essential to remark that the coolant conductivity is constant (~1 $\mu S/cm^2$) for the presented test matrix. This figure shows the operating points that had not been measured and the reason behind this. Some ambient conditions were not reachable by the testbed, and others were not possible due to the warm weather conditions during the measuring time. Fig. 5B shows the measured polarization curves. This plot illustrates the variability in the obtained data. In the present figure, the dots represent each of the 15 steps of the polarization curve experimental protocol. The dashed lines are used to mark the polarization curve of each set of 15 dots. The solid lines are used to mark the maximum and minimum values of the system. This aesthetic way of representing the obtained data will be used throughout the paper. This representation is used for Figs. 5, 6, 15, 16, 17, 18, and 19.

This figure shows in a general way that the variation in the ambient operating conditions changes the performance of the FC. In idle, the voltage difference is 2.2 V (1.07%), which is not very significant. The current control of the facility has a small uncertainty that could influence this result. For example, the idle state current value is 62.5 A, but the real produced value has a maximum of 63.5 A and minimum of 62.88 A; this means there is always a device-induced error related to the facility (~1.6%). However, as the current grows, the change in voltage due to the operating conditions becomes larger, reaching its maximum at a 5.4 V difference (3.3% variation in the stack voltage). Thus, the performance difference at high currents is not a measuring error and is produced by the change in the ambient operating conditions. This is done in Section 3.1.1 for the relative humidity and in Section 3.1.2 for the stack temperature.

The power distribution along the polarization curve shows the same trend (Fig. 6). The performance of the FC does not change with the operating conditions in idle, but it becomes sensitive to them as the current increases, reaching a maximum variability of 3.68%. It is important to remark that this change in voltage is not caused by an error in the established current, since its uncertainty is around 0.3%. The presented figures show a general deviation in the results. However, the polarization curves under different conditions of relative humidity and temperature should be isolated to analyze the influence of ambient conditions.

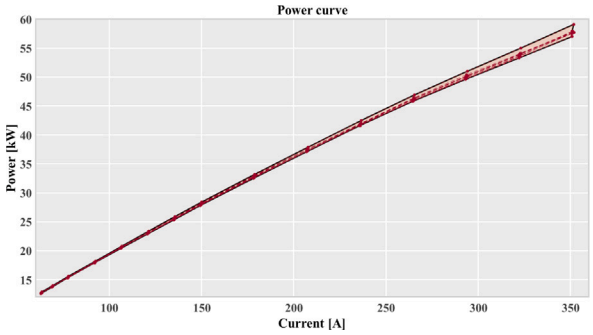

Fig. 6. Stack power along the polarization curve in different operating conditions.

3.1.1. Influence of ambient relative humidity in the FC performance

The results produced during the first part of the experimental campaign have been grouped to produce equal-temperature datasets. Fig. 7 shows three different temperatures (20 °C, 30 °C, and 40 °C) where the relative humidity has been changed. This figure clearly shows for the three sets of data that when the ambient relative humidity increases the performance of the FC improves. The performance improvement can be noted in the increment of voltage produced by the same current level when there is higher relative humidity. This change in the voltage level leads to higher power production.

The performance decay with low humidity is a known phenomenon in FC and many authors are currently looking into a way to solve it [48]. However, When studying carefully the humidity-related performance improvement, it can also be noted that this effect increases with the current. At high load the effect of humidity is more important, being 2.5 V (around 2%) the highest difference achieved (20 °C, from 65% to 80% relative humidity). At higher currents, the air mass flow needed to produce current is larger, which means the humid air that flows into the cathode and thus the amount of water introduced is also larger, which is a possible reason for the performance improvement.

Nevertheless, the open cathode geometry is a remarkable characteristic of the FC that should be considered. The open cathode geometry at low currents tends to produce local membrane dehydration [49]. The air supply directly from the ambient to the open cathode can be a challenging process that may produce an uneven water distribution in the membrane, which worsens the FC performance. As the current increases, the amount of water produced in the electrochemical reaction also increases, rapidly spreading along the membrane and providing a good hydration level. This may explain the reason behind the performance improvement at higher currents and the high influence of humidity in this kind of FC stack. Thus, these results show that, in contrast to other cell geometries in which humectation is not needed [50], an open cathode would benefit in a significant way from the presence of a humidifier in the system.

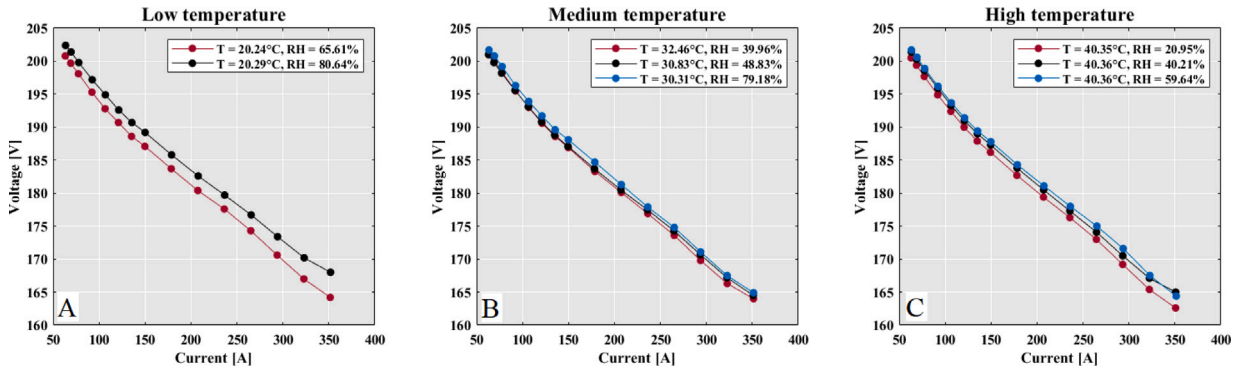

Fig. 7. Effect of humidity on the polarization curve. (A) Low temperature data (20 °C). (B) Medium temperature data (30 °C). (C) High temperature data (40 °C).

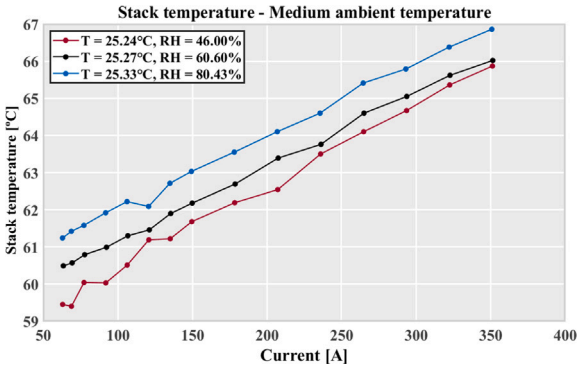

Fig. 8. Relation of the stack temperature with ambient relative humidity.

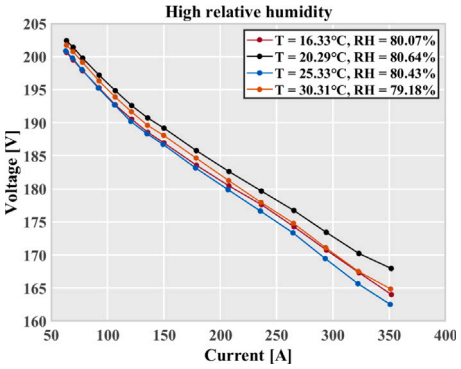

Fig. 9. High humidity and variable temperature polarization curves.

Leaving aside the peculiarities of the open cathode geometry, the performance improvement with humidity has other explanations. The proton conductivity of the membrane highly depends on its humidity level. A dry membrane is less conductive, but too much water can flood the membrane and block the membrane making the proton exchange process harder. In addition, subjecting the membrane to dry conditions causes its rapid degradation.

The studied FCS has a relatively high idle current value of 62.5 A. The reason behind this may be due to the previously-mentioned reasons. A higher idle current could lead to avoiding an uneven water distribution in low current conditions or high voltage operation leading to fast degradation, thus, keeping the membrane safe from the risks of these conditions.

The study of any condition influencing the performance of the FCS should consider its impact on the control parameters of the system. As it has previously been explained, the temperature of the stack is a key parameter in the correct functioning of the FC. Fig. 8 shows the influence of relative humidity in this parameter. It can be noted when the cathode inlet relative humidity increases, the temperature of the stack rises. This result makes sense according to what has already been explained about humidity in the membrane. The increase in the stack temperature may be a correcting effect to heat the stack and avoid flooding in the membrane as this gets more humid, but further data or 3D-CFD simulations would be required to provide a definite conclusion.

Finally, the study of other parameters such as the compressor power does not have any direct relation with the relative humidity. The calculation of the specific humidity or water content of the inlet does not provide additional information, it shows the same trend as the relative humidity.

3.1.2. Influence of temperature in the FC performance

The produced results are now grouped in equal-humidity sets to permit the analysis of the influence of ambient temperature in the polarization curve (Fig. 9). In this case, the humidity control is hard to stabilize, therefore there is a maximum uncertainty (~5%) in the relative humidity establishment. The sets of equal-relative humidity data have been grouped considering this deviation and computing the average value of the ambient relative humidity measurements.

In this case, the equal-relative humidity sets show no clear relation between the ambient temperature of the air and the polarization curve change. Fig. 9 is used to show that there is no clear trend in the results. Theoretically, the temperature of the air that goes into the system in an open cathode design should have an impact on the performance of the stack. As water distribution represents an essential challenge in an open cathode, at low currents, high temperatures remove too much water from the system and increase the risk of drying the membrane. In contrast, at high currents, high temperatures should ease the removal of water that accumulates and could flood the membrane. However, Fig. 9 makes it clear that there is no direct trend that relates air inlet temperature with performance. The reason behind this may be that the design of this FC protects itself from the dangers of variable temperature on the stack with the control strategy of the cooling circuit. As the stack temperature is a critical parameter in the performance of an FCS, its control allows not only higher efficiencies, but also a safer and more stable performance for the membrane [51]. Fig. 3 shows a precise temperature control in the stack, performed by the ECU of the FCS. Each temperature is regulated with its own calibrated PID that uses the cooling system of the FCS to achieve a specific value that provides the optimal performance for each current. Thus, as it can be seen in Fig. 1, the flow that goes into the system is not in the same thermodynamic conditions as that entering the FCS since it passes first through the compressor and then through a heat exchanger that modifies its temperature.

It is well-known that the temperature of the membrane influences its properties and performance, but it also plays an important role in its degradation process. The best performance is usually found between

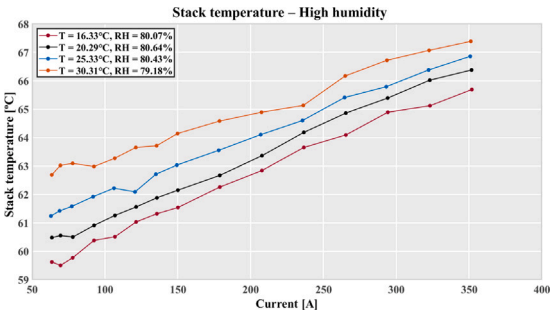

Fig. 10. Relation of the stack temperature with ambient temperature.

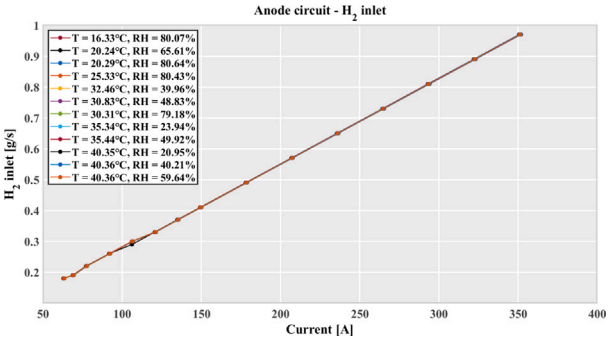

Fig. 11. H_2 that flows into the system in each step of the polarization curve.

75 °C and 80 °C, but high temperatures can damage the membrane, this may be the reason behind the lower temperatures in Fig. 10. In this figure, it is easy to note that the temperature of the stack increases with the ambient temperature since the FC stack and the cooling circuit placed in the testing room are exchanging heat with the environment which is at a higher temperature.

In conclusion, the air inlet temperature in this FCS is not directly related to the polarization curve due to the cooling circuit control. Nevertheless, it could have an indirect relation with the performance of the system. The temperature could influence the air mass flow into the cathode: fraction of water, compressor power needed, and ease of the electrochemical reaction. This indirect relation is studied in detail in Section 3.3.

3.2. Anode circuit: H_2 consumption

In an FCS, the generation of electric current comes from the electrochemical reaction between H_2 and O_2. Thus, the consumed reactants must be studied to understand the obtained polarization curve.

On the one hand, the H_2 value that can be measured with the existing facility is the mass flow in the FCS anode inlet. Fig. 11 shows that the mass flow of H_2 that goes into the anode system is a fixed value for each current and is independent of what happens in the cathode circuit. However, this inlet mass flow ($\dot{m}_{H_2}$) is not the same amount of H_2 used in the current production ($\dot{m}_{H_{2_{curr}}}$). The H_2 mass flow is divided into current generation, purged, and crossover losses (Eq. (1)). Furthermore, in Fig. 1 it can also be noted that a passive recirculation system allows the H_2 mass flow to always be at the right pressure conditions. Understanding the distribution between the three H_2 flows allows us to know in which way H_2 losses influence the efficiency of the system.

$$\dot{m}_{H_2} = \dot{m}_{H_{2_{curr}}} + \dot{m}_{purged} + \dot{m}_{crossover} \tag{1}$$

The amount of H_2 used in the current generation is easy to estimate considering the two electrons per mole of H_2, the known Faraday constant, the current generated, and the molar mass of H_2 (Eq. (2)).

$$\dot{m}_{H_{2_{curr}}} = \frac{N \cdot I}{2 \cdot F} \cdot M_{H_2} \tag{2}$$

The H_2 crossover mass flow refers to the H_2 that passes from the anode to the cathode through the membrane and, thus, is not used in the current generation. This is an undesired phenomenon and it produces a loss in the FC efficiency. The crossover losses are related to the H_2 anode pressure and are not influenced by the conditions in the cathode. Due to confidentiality reasons, it is not possible to disclose information about the anode pressure of the present FCS. However, following the models presented in [52] an approximation of the current lost by the H_2 crossover can be obtained about the anode pressure. This current value allows us to obtain an approximation of the diffused H_2 by following Eq. (3).

$$\dot{m}_{crossover} = \frac{N \cdot I_{crossover}}{2 \cdot F} \cdot M_{H_2} \tag{3}$$

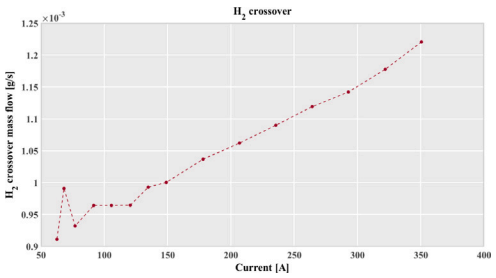

Fig. 12. H_2 crossover mass flow estimation.

Taking the average value for each current step, a rough estimation of the H_2 crossover mass flow is presented in Fig. 12. The obtained crossover mass flows are insignificant concerning the inlet H_2 mass flow for each current. This mass flow represents around a 0.5% of the H_2 in the anode circuit. Thus, this small mass flow may have an impact on the efficiency of the system, but its main problem is how this undesired H_2 diffusion affects the membrane. It has been proved [53] that pinholes appear around the H_2 diffusion path. The formation of pinholes facilitates the crossover of more particles and creates areas in which H_2 and O_2 mix at the cathode. The reaction between these two gases produces combustion and, thus, heat release or temperature differences in the membrane [54]. The produced heat in the cathode causes thinning in the membrane, which accelerates its degradation. In addition, H_2 crossover also accelerates the chemical degradation of the membrane due to the production of free H_2 radicals (H*) that attack the carbon in the membrane. Therefore, the crossover phenomenon is important due to its damaging side effects on the membrane rather than its mass flow consumption.

Once the inlet H_2, crossover and current generation mass flows are known, it should be easy to obtain the amount of H_2 that is purged from the system. The problem is that the precision of the equipment when measuring the inlet H_2 is too low (one decimal). Therefore, it is not possible to compare the H_2 mass flow inlet with the current computed value, which would have a higher number of decimals. To understand the H_2 consumption process, in this case, the transient recorded data is more appropriate. The performance of the HyTron is not completely steady and it feeds a different mass flow in each time instant. In addition, the established current also has an associated error. Fig. 13 shows the inlet H_2 mass flow ($\dot{m}_{H_2}$), the current generation mass flow ($\dot{m}_{curr}$) and the computed average of $\dot{m}_{H_2}$ in each current step ($\overline{m}_{H_2}$). Theoretically, $\overline{m}_{H_2}$ should be greater than $\dot{m}_{curr}$, as stated in (1). Nevertheless, in Fig. 13 it can be noted that, at some current steps, $\dot{m}_{curr}$ can be higher than $\overline{m}_{H_2}$.

The high oscillations in $\dot{m}_{H_2}$ that can be seen in 13 represent the opening and closing of the purging valve. A high amount of H_2 goes

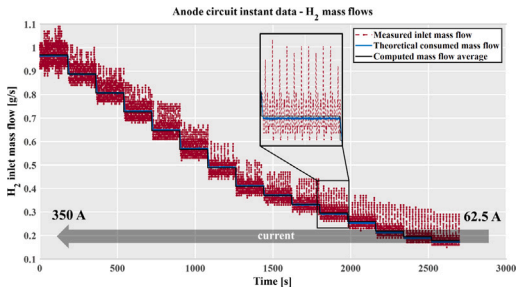

Fig. 13. Instant data of the H_2 inlet in the polarization curve test.

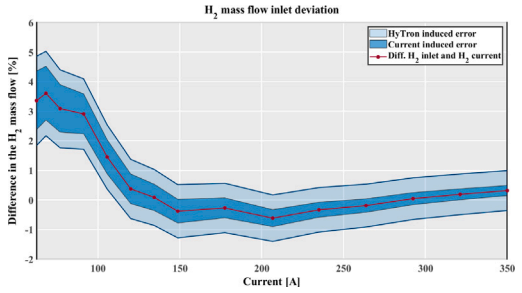

Fig. 14. Difference between the H_2 mass flow measured at the inlet and the theoretical mass flow that would be consumed in the current generation process.

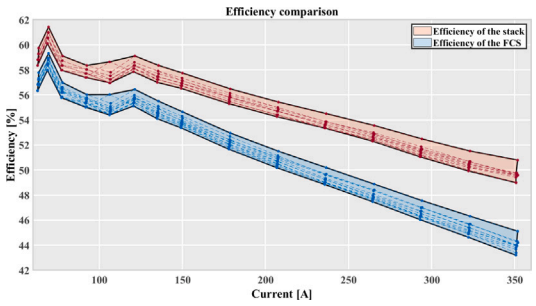

Fig. 15. Efficiency of the FC stack module and FCS.

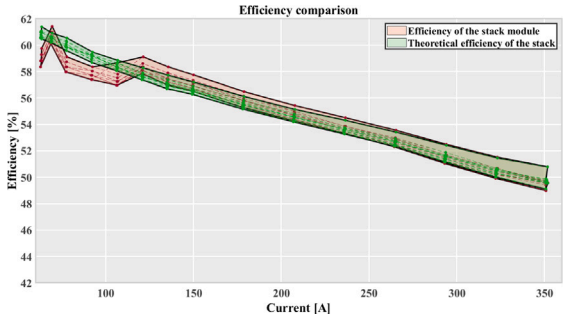

Fig. 16. Efficiency of the FC stack module and its theoretical value.

into the system and then, the purging valve opens to eliminate the N_2 gas that has crossed the membrane through diffusion. It can be observed that, at high currents, the mass flow that goes into the system and the one that goes out by the purge is significantly higher than at low loads. A possible reason behind this effect is that at high currents the partial pressure of N_2 in the cathode increases, thus increasing its diffusion through the membrane, thus, the purging process must occur more frequently. The amount of H_2 that goes into the system is higher than the amount needed so that the flow that goes out in the purge can be larger and let the highest amount of anode gas possible clean from other gases. This is reflected in Fig. 13 since at high currents, the time step between purges (~3 s) is smaller than at low currents (~8 s). At high currents, the purging valve opens with higher frequency so that the N_2 gas do not accumulate in the membrane.

To observe the deviation between H_2 flows more clearly, the difference between values can be observed in Fig. 14 for one specific test in standard conditions (25 °C and 65% of relative humidity). This figure shows one of the experimental tests, but the trend observed in this image is the same in all of the performed tests.

It is interesting to note that, at high load, the difference between the average FCS H_2 consumption ($\overline{m}_{H_2}$) and $\dot{m}_{curr}$ is very small, up to 0.6%. This small deviation probably comes from the addition of all the different errors acting on the measurement process. It should be remarked that the current establishment has an associated error, and this value is used by the ECU to select the H_2 inlet. Moreover, the HyTron device also has its technical error associated with performance. Thus, it is expected to have some uncertainties in the mass flow of H_2 that goes into the system at each time instant. The extent of these technical errors is represented by the volumes in Fig. 14.

Fig. 14 also shows that at low loads the amount of H_2 that flows into the system concerning the current-required mass flow, increases significantly. Two increments repeat consistently in every performed test, first a ~1.5% increase at the 105.6 A step and then, again at lower currents (~3% deviation from the theoretical current mass flow value). These observed H_2 increments are not technical errors from the devices, they correspond to the H_2 supply strategy chosen by the FCS.

When analyzing in deep detail the obtained data, it can be noted that both the anode and cathode pressures should increase with the current. At low loads, the amount of H_2 going into the system is higher than the one needed to produce the desired current, which triggers higher H_2 purge rate. This H_2 excess results in a worse H_2 utilization.

The efficiency of the energy production in the module (stack + anode circuit) comes from the ratio between the power generated and the power that, theoretically, the inlet H_2 mass flow could produce (Eq. (4)).

$$\eta_{module} = \frac{P_{FC}}{\dot{m}_{H_2} \cdot LHV} \tag{4}$$

However, the efficiency of the module is not representative of the whole system. The efficiency of the FCS considers the module and its related BoP consumption. Thus, the efficiency of the FCS is presented in Eq. (5).

$$\eta_{FCS} = \frac{P_{FC} - P_{BoP}}{\dot{m}_{H_2} \cdot LHV} \tag{5}$$

Both values are presented in Fig. 15. This image shows that the maximum FCS efficiency is close to 60%, the usual maximum efficiency value for this kind of powertrain. This maximum value is reached at low loads, around 20% of the nominal power the FCS can produce. This result is appropriate for the studied FCS because this powertrain would mainly be used coupled with other FCS in a modular way for HDFCV. Moreover, it coincides with the expected performance. At low loads, the smaller BoP consumed power allows a higher efficiency. The obtained plot shows a drop in the low current efficiencies, but this follows the tendencies seen in different literature sources [55].

When calculating the η_{module} using the theoretical H_2 mass flow the FC would require to produce the desired current, the result is slightly different. In this case, the tendency is linear and decreases from minimum to maximum current (Fig. 16). This means the observed η_{module} drop is related to the H_2 mass flow strategy of the FCS.

The chosen H_2 supply strategy supplies an excess of reactant into the anode and has an associated uncertainty. This produces an efficiency drop but also provides two operating points in which the efficiency is higher than in the theoretical case when the uncertainty introduced by

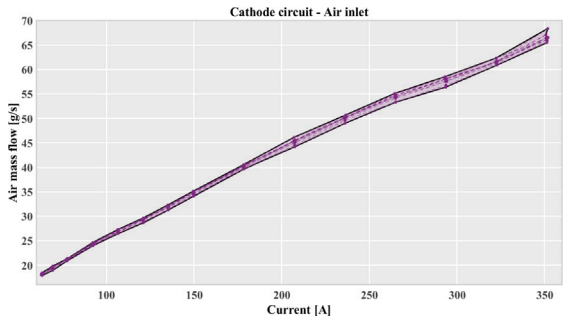

Fig. 17. Air inlet into the cathode circuit.

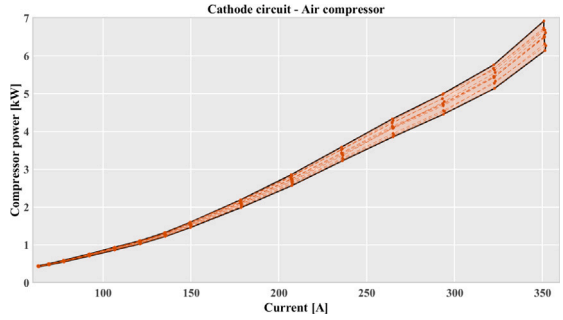

Fig. 18. Power consumed by the compressor along the polarization curve.

the Hytron produces H_2 consumption values that are lower than those calculated from the current. Considering the stationary conditions in which this FCS mainly operates, this is an important advantage for its performance.

3.3. Cathode circuit: O_2 consumption

Once the anode circuit has been studied in detail, the analysis of the cathode or air circuit will allow the understanding of the processes taking place in this FCS. The O_2 used in the electrochemical reaction comes from the air that flows into the cathode inlet and is measured by the Flowsonix device. Fig. 17 shows that the air that comes from the Flowsonix depends on the ambient conditions. The differences in temperature and relative humidity together with pressure variations modify the properties of the air, such as its density, which produces a variation in the inlet flow. This variation becomes greater as the current increases, reaching a maximum of 4.4% difference between values at maximum load.

Producing higher power requires more reactant, thus, a higher amount of air flows into the cathode. However, this means the compressor admits more air and consumes more power. The 4.4% of air mass flow difference produces a 12.73% difference in the power consumed by the compressor at maximum load (Fig. 18), which is quite significant and could highly be affecting the efficiency of the system, as seen in Fig. 15.

However, when analyzing the performance of the cathode circuit, it is important to study the relation between the inlet and the consumed species, the stoichiometry. It is not possible to measure the consumed oxygen, but this value can be estimated by the produced current and the amount of air required to supply it. Thus, Eq. (6) is used to calculate the cathode stoichiometry.

$$\dot{m}_{air_{feed}} = \frac{I \cdot N}{4 \cdot F \cdot x_{O_2}} \cdot \lambda_{cathode} \cdot M_{air} \tag{6}$$

The data obtained from this calculation is quite significant for the processes happening inside the FCS. In Fig. 19, it can be noted

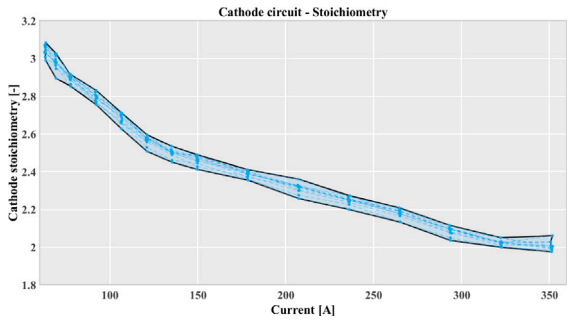

Fig. 19. Air inlet into the cathode circuit.

that ambient conditions influence the cathode stoichiometry, as in the previously studied FCS parameters. However, in this case, the variation in the results does not depend on the current, it is always between 3% and 5%. This means that the cathode circuit has an inlet strategy based on the stoichiometry for each current rather than the air mass flow. The air inlet is variable due to the ambient conditions that change its density.

Fig. 19 shows that the cathode stoichiometry ranges from ~2 to ~3, which are in the usual value range. Typically, when the mass flow inlet consists of pure O_2, the cathode stoichiometry ranges between 1.2 and 1.5 [56]. However, when the mass flow that goes into the cathode is air, the usual value is 2 or higher but can be reduced slightly to maximize the FCS performance. The stoichiometry increase has a positive effect on the performance of the FC stack [57]. In fact, the benefits of improving air inlet control have turned this issue into a significant research matter [58,59]. A higher air mass flow inside the cathode implies a larger concentration of O_2 available for the electrochemical reaction, thus, a higher efficiency of the process. In addition, a higher flow rate in the cathode eases the water removal in the cell. The problem with the air excess is that the flow into the cathode uses an air compressor. Any increase in the air mass flow comes together with a power demand increase from the compressor. This BoP power (Fig. 18) is significant and cannot be neglected, as it was observed in Fig. 15 it has an important impact on the efficiency of the system. When the power produced by the FCS is low, the compressor operates with low pressure-ratio and mass flow rate, thus the BoP power consumption is low and has small impact on the efficiency of the FCS (Fig. 19).

4. Potential for industrial applications

The performed study aims to understand the influence of the operating conditions on the steady-state performance of an FCS for HDV applications. As this represents a topic of interest in the current research [60]. Operating conditions include temperature and relative humidity of the air that goes into the system, thus, this study analyzes the impact of different weather conditions in an FCS. The understanding of the influence of the weather in the operation of the system can be very interesting for the manufacturer of this kind of powertrain. The obtained results for the open cathode geometry show that relative humidity influences the power generation processes. Thus, the it may be interesting to consider studying this influence in deeper detail and study in detail the influence of including a humidifier in the system, which is a current subject of interest [61].

Additionally, the obtained data about the inlet gases, both anode and cathode, can be very useful in the optimization process of FCS. The shown transient H_2 inlet data helps to understand the efficiency of the system along the polarization curve and is very valuable in its future improvement. Considering the development stage of this kind of propulsive system, having a dataset with this level of detail is quite significant in its understanding.

Furthermore, the acquired data about the compressor power related to the stoichiometry of the cathode is also valuable for manufacturers. This allows them to understand how the air mass flow or cathode circuit could be improved for this specific open cathode geometry.

All these sensitivity analyses serve to inform the scientific community and the industry about how the performance of FCS vary with the operating conditions, thus minimizing the need for extensive and expensive experimental campaigns until the last phases of the FCS design. Therefore, the use of these trends may assist the FCS technology development process, thus accelerating the implementation of such technologies in the transportation sector. The experimental activity findings provide some qualitative information about the performance of the system that may be useful. Nonetheless, it is important to acknowledge the significance of the numerical values on its own. These values allow building an FCS database that is critical in the development of simulation models with a high level of detail.

5. Conclusion

The present study represents a significant contribution to the existing literature shown in Section 1 due to its novelty. As explained before, in the available information in the literature there exists no dedicated paper that studies in detail the effect of changing the operating conditions in a state-of-the-art FCS. In addition, there are few experimental studies about FCS and, even less, using specific FCS designed for HDV for this study. The performed analysis reviews in deep detail all the significant parameters in the energy production process (anode, cathode and BoP power), whereas, other literature studies focus on the polarization curve or other current profiles leaving aside the gas supplies or other parameters involved in the process, as explained in Section 1. Additionally to its main objective of analyzing the steady-state performance of the FCS, the present study also gives insight into the instantaneous control done by the ECU of the system. Fig. 13 gives an idea about how the purging process of the FCS works to provide the most appropriate performance for the existing open cathode geometry of the cells.

This work has successfully generated results about the steady-state performance of a 60 kW FCS. The obtained set of data is highly valuable for both the industry and the currently open research topics and allows a better understanding and characterization of this kind of powertrain.

The analysis of the results leads to the obtention of the following conclusions:

- A higher ambient relative humidity improves the performance of the FCS. This influence of the air humidity becomes more significant as the current increases. However, the temperature of the air inlet does not seem to have a direct impact on the performance of the FCS.
- The study of the anode circuit has shown that this FCS supplies an excess of H_2 at low currents. In terms of FCS performance, this translates into an increase in efficiency at some specific currents. Any variation in the ambient conditions has no impact on the H_2 demand, which is controlled by the supply current only.
- The cathode analysis shows the air inlet strategy is a stoichiometry-based control selected by the current of the FCS. Ambient conditions have a small influence on the air inlet, but they mainly affect the power demanded by the compressor.
- The obtained set of data is representative of the functioning of a 60 kW FCS. This database contains information about the variations produced by the ambient conditions along the polarization curve. The acquisition of this kind of result facilitates the modeling of a realistic FCS model. These results show in detail the performance of the system as they not only include the power generated but also the inlet gases, BoP power, and efficiency of the system.

It is important to remark that, the experimental activities that have been carried out for this study represent a fraction of what can be tested with this facility. The present study aims to set the basis for the characterization of the system, which will lead to future experimental campaigns.

CRediT authorship contribution statement

Jose M. Desantes: Supervision, Project administration, Conceptualization. **R. Novella:** Supervision, Resources, Project administration, Methodology, Formal analysis. **M. Lopez-Juarez:** Writing – review & editing, Software, Resources, Methodology, Investigation, Data curation. **I. Nidaguila:** Writing – original draft, Validation, Methodology, Investigation, Conceptualization.

Declaration of competing interest

The authors declare that they have no known competing financial interests or personal relationships that could have appeared to influence the work reported in this paper.

Data availability

Data will be made available on request.

Acknowledgments

This research has been partially funded by Universitat Politècnica de València through the support program for research and development (PAID-01-22) and was performed in the frame of the ALL-IN Zero project, which is funded by the European Union's Horizon Europe research and innovation program under grant agreement N^o 101069888. Funding for open access charge: CRUE-Universitat Politècnica de València.

References

[1] Intergovernmental Panel on Climate Change (IPCC). Summary for policymakers. In: Global warming of 1.5° C. Cambridge University Press; 2022, http://dx.doi.org/10.1017/9781009157940.001.
[2] European Comission. A green deal industrial plan for the net-zero age. Tech. rep, Brussels; 2023.
[3] International Energy Agency (IEA). Energy technology perspectives 2017. Tech. rep, Paris; 2017.
[4] International Energy Agency (IEA). Technology roadmap hydrogen and fuel cells. Tech. rep, Paris; 2015.
[5] Venkata KoteswaraRao K, Naga Srinivasulu G, Ramesh Rahul J, Velisala V. Optimal component sizing and performance of Fuel Cell – Battery powered vehicle over world harmonized and new european driving cycles. Energy Convers Manage 2024;300:117992. http://dx.doi.org/10.1016/j.enconman.2023.117992.
[6] Study on hydrogen substitution in a compressed natural gas spark-ignition passenger car engine. Energy Convers Manage 2023;291:117259. http://dx.doi.org/10.1016/j.enconman.2023.117259.
[7] Longden T, Beck FJ, Jotzo F, Andrews R, Prasad M. 'Clean' hydrogen? – Comparing the emissions and costs of fossil fuel versus renewable electricity based hydrogen. Appl Energy 2022;306:118145. http://dx.doi.org/10.1016/j.apenergy.2021.118145.
[8] Desantes J, Molina S, Novella R, Lopez-Juarez M. Comparative global warming impact and NOX emissions of conventional and hydrogen automotive propulsion systems. Energy Convers Manage 2020;221:113137. http://dx.doi.org/10.1016/j.enconman.2020.113137.
[9] The Emissions Database for Global Atmospheric Research (EDGAR). Annual greenhouse gas (GHG) emissions worldwide from 1990 to 2022, by sector (in million metric tons of carbon dioxide equivalent). Tech. rep, Joint Research Center (JRC); 2023.
[10] The Emissions Database for Global Atmospheric Research (EDGAR). Distribution of carbon dioxide emissions worldwide in 2022. Tech. rep, Joint Research Center (JRC); 2023.
[11] International Energy Agency (IEA). Distribution of carbon dioxide emissions produced by the transportation sector worldwide in 2022, by sub sector. Tech. rep, 2023.

[12] Pardhi S, Chakraborty S, Tran D-D, El Baghdadi M, Wilkins S, Hegazy O. A review of fuel cell powertrains for long-haul heavy-duty vehicles: Technology, hydrogen, energy and thermal management solutions. Energies 2022;15(24). http://dx.doi.org/10.3390/en15249557.

[13] Zhu P, Mae M, Matsuhashi R. Techno-economic analysis of grid-connected hydrogen production via water electrolysis. Energies 2024;17(7). http://dx.doi.org/10.3390/en17071653.

[14] María Villarreal Vives A, Wang R, Roy S, Smallbone A. Techno-economic analysis of large-scale green hydrogen production and storage. Appl Energy 2023;346:121333. http://dx.doi.org/10.1016/j.apenergy.2023.121333.

[15] Burke AF, Zhao J, Miller MR, Sinha A, Fulton LM. Projections of the costs of medium- and heavy-duty battery-electric and fuel cell vehicles (2020–2040) and related economic issues. Energy Sustain Dev 2023;77:101343. http://dx.doi.org/10.1016/j.esd.2023.101343.

[16] Ananda S, Mulholland E, Musa A. Race to zero European heavy-duty vehicle market development quarterly (January–December 2023). ICCT; 2024.

[17] Piras M, De Bellis V, Malfi E, Novella R, Lopez-Juarez M. Hydrogen consumption and durability assessment of fuel cell vehicles in realistic driving. Appl Energy 2024;358:122559. http://dx.doi.org/10.1016/j.apenergy.2023.122559.

[18] Novella R, la Morena JD, Lopez-Juarez M, Nidaguila I. Effect of differential control and sizing on multi-FCS architectures for heavy-duty fuel cell vehicles. Energy Convers Manage 2023;293:117498. http://dx.doi.org/10.1016/j.enconman.2023.117498.

[19] Piras M, De Bellis V, Malfi E, Desantes JM, Novella R, Lopez-Juarez M. Incorporating speed forecasting and SOC planning into predictive ECMS for heavy-duty fuel cell vehicles. Int J Hydrog Energy 2024;55:1405–21. http://dx.doi.org/10.1016/j.ijhydene.2023.11.250.

[20] Nurdin HI, Benmouna A, Zhu B, Chen J, Becherif M, Hissel D, Fletcher J. Maximum efficiency points of a proton-exchange membrane fuel cell system: Theory and experiments. Appl Energy 2024;359:122629. http://dx.doi.org/10.1016/j.apenergy.2024.122629.

[21] Pacheco C, Barbosa R, Ordoñez L, Sierra J, Escobar B. Design, simulation and experimental characterization of a high-power density fuel cell. Int J Hydrog Energy 2021;46(51):26197–204. http://dx.doi.org/10.1016/j.ijhydene.2021.01.132, XIX Mexican Hydrogen Society Congress Special Issue.

[22] Neto RC, Teixeira JC, Azevedo J. Thermal and electrical experimental characterisation of a 1 kW PEM fuel cell stack. Int J Hydrog Energy 2013;38(13):5348–56. http://dx.doi.org/10.1016/j.ijhydene.2013.02.025.

[23] Qiu F, Sun Z, Li H, Ahad Y. Design of a novel low-temperature polymer electrolyte Membrane fuel Cell: 3D modelling and experimental verification. Appl Therm Eng 2024;236:121480. http://dx.doi.org/10.1016/j.applthermaleng.2023.121480.

[24] Ren G, Qu Z, Wang X, Zhang G, Wang Y. Electrospun fabrication and experimental characterization of highly porous microporous layers for PEM fuel cells. Int J Hydrog Energy 2024;55:455–63. http://dx.doi.org/10.1016/j.ijhydene.2023.11.226.

[25] Tang W, Chang G, Xie J, Shen J, Pan X, Yuan H, Wei X, Dai H. A comprehensive investigation on performance heterogeneity of commercial-size fuel cell stacks during dynamics operation. Energy Convers Manage 2024;301:117998. http://dx.doi.org/10.1016/j.enconman.2023.117998.

[26] Hou Y, Schall J, Dietze S, Kurz T, Gerteisen D. An experimental and numerical study of spatial and temporal catalyst degradation during start-up and shut-down of PEM fuel cells. J Power Sources 2024;591:233780. http://dx.doi.org/10.1016/j.jpowsour.2023.233780.

[27] Tao J, Wei X, Wang X, Jiang S, Dai H. Control-oriented cold start modelling and experimental validation of PEM fuel cell stack system. Int J Hydrog Energy 2024;50:450–69. http://dx.doi.org/10.1016/j.ijhydene.2023.08.240.

[28] Dirkes S, Leidig J, Fisch P, Pischinger S. Prescriptive lifetime management for PEM fuel cell systems in transportation applications, part II: On-board operando feature extraction, condition assessment and lifetime prediction. Energy Convers Manage 2023;283:116943. http://dx.doi.org/10.1016/j.enconman.2023.116943.

[29] Placca L, Kouta R, Candusso D, Blachot J-F, Charon W. Analysis of PEM fuel cell experimental data using principal component analysis and multi-linear regression. Int J Hydrog Energy 2010;35(10):4582–91. http://dx.doi.org/10.1016/j.ijhydene.2010.02.076, Novel Hydrogen Production Technologies and Applications.

[30] Zhang B, Wang X, Gong D, Xu S. Experimental analysis of the performance of the air supply system in a 120 kW polymer electrolyte membrane fuel cell system. Int J Hydrog Energy 2022;47(50):21417–34. http://dx.doi.org/10.1016/j.ijhydene.2022.04.189.

[31] Okech G, Emam M, Mori S, Ahmed M. Experimental study on the effect of new anode flow field designs on the performance of direct methanol fuel cells. Energy Convers Manage 2024;301:117988. http://dx.doi.org/10.1016/j.enconman.2023.117988.

[32] Meng X, Ren H, Xie F, Shao Z. Experimental study and optimization of flow field structures in proton exchange membrane fuel cell under different anode modes. Int J Hydrog Energy 2023;48(63):24447–58. http://dx.doi.org/10.1016/j.ijhydene.2023.03.229.

[33] Meng X, Ren H, Yang X, Tao T, Shao Z. Experimental study of key operating parameters effects on the characteristics of proton exchange membrane fuel cell with anode recirculation. Energy Convers Manage 2022;256:115394. http://dx.doi.org/10.1016/j.enconman.2022.115394.

[34] Weng F-B, Dlamini MM, Tirumalasetti PR, Hwang J-J. Experimental evaluation of flow field design on open-cathode proton exchange membrane fuel cells (PEMFC) short stack consisting of three cells. Renew Energy 2024;226:120411. http://dx.doi.org/10.1016/j.renene.2024.120411.

[35] Chang H, Cai F, Yu X, Duan C, Chan SH, Tu Z. Experimental study on the thermal management of an open-cathode air-cooled proton exchange membrane fuel cell stack with ultra-thin metal bipolar plates. Energy 2023;263:125724. http://dx.doi.org/10.1016/j.energy.2022.125724.

[36] Desantes J, Novella R, Pla B, Lopez-Juarez M. A modeling framework for predicting the effect of the operating conditions and component sizing on fuel cell degradation and performance for automotive applications. Appl Energy 2022;317:119137. http://dx.doi.org/10.1016/j.apenergy.2022.119137.

[37] Lopez-Juarez M, Rockstroh T, Novella R, Vijayagopal R. A methodology to develop multi-physics dynamic fuel cell system models validated with vehicle realistic drive cycle data. Appl Energy 2024;358:122568. http://dx.doi.org/10.1016/j.apenergy.2023.122568.

[38] Kölbl J, Ferrara A, Hametner C. Impact of energy management strategy calibration on component degradation and fuel economy of heavy-duty fuel cell vehicles. IFAC-PapersOnLine 2022;55(24):317–22. http://dx.doi.org/10.1016/j.ifacol.2022.10.303, 10th IFAC Symposium on Advances in Automotive Control AAC 2022.

[39] Booto GK, Aamodt Espegren K, Hancke R. Comparative life cycle assessment of heavy-duty drivetrains: A norwegian study case. Transp Res D 2021;95:102836. http://dx.doi.org/10.1016/j.trd.2021.102836.

[40] Morizet N, Desforges P, Geissler C, Pahon E, Jemei S, Hissel D. An adaptative approach for estimating the remaining useful life of a heavy-duty fuel cell vehicle. J Power Sources 2024;597:234152. http://dx.doi.org/10.1016/j.jpowsour.2024.234152.

[41] Yang YH, Lin Q, Zhang CF, Li GQ. Study of the influence under different operating conditions on the performance of hydrogen fuel cell system for a bus. Process Saf Environ Prot 2023;177:1027–34. http://dx.doi.org/10.1016/j.psep.2023.07.044.

[42] Desantesa JM, Novella R, Lopez-Juarez M, Nidaguila I. Comparative analysis of powertrain architectures for fuel cell light commercial vehicles in terms of performance, durability, and environmental impact. In: FISITA world congress 2023. 2023, http://dx.doi.org/10.46720/fwc2023-ppe-039.

[43] Green Car Congress. Stellantis developing hydrogen fuel cell light commercial vehicle; partnership with Faurecia and Symbio. 2021.

[44] Gerring G. AVL facility engineering, system integration & turnkey handbook. Tech. rep, AVL Iberica SA - Turnkey and Facility Engineering; 2017.

[45] AVL. Solution sheet AVL FLOWSONIX AIR. Tech. rep, AVL List GmbH; 2018.

[46] AVL. AVL ConsysCool 200 coolant conditioning system - product guide. Tech. rep, AVL List GmbH; 2018.

[47] Kabza A, Malkow T, Antoni L, Muñoz M, Tsotridis G, Pilenga A, Schätzle M, Rosini S, Van Bogaert G, Thalau O, Bove R, Honselaar M, De Marco G. PEFC power stack performance testing procedure – Measuring voltage and power as function of current density. Polarisation curve test method. test module PEFC ST 5-3. Joint Research Centre Publications Office; 2010, http://dx.doi.org/10.2790/18880.

[48] Wang Y, Xu H, Wang X, Gao Y, Su X, Qin Y, Xing L. Multi-sub-inlets at cathode flow-field plate for current density homogenization and enhancement of PEM fuel cells in low relative humidity. Energy Convers Manage 2022;252:115069. http://dx.doi.org/10.1016/j.enconman.2021.115069.

[49] Yang Y, Jia H, Liu Z, Bai N, Zhang X, Cao T, Zhang J, Zhao P, He X. Overall and local effects of operating parameters on water management and performance of open-cathode PEM fuel cells. Appl Energy 2022;315:118978. http://dx.doi.org/10.1016/j.apenergy.2022.118978.

[50] Penga Ž, Bergbreiter C, Barbir F, Scholta J. Numerical and experimental analysis of liquid water distribution in PEM fuel cells. Energy Convers Manage 2019;189:167–83. http://dx.doi.org/10.1016/j.enconman.2019.03.082.

[51] Yu X, Liu Y, Tu Z, Chan SH. Endplate effect in an open-cathode proton exchange membrane fuel cell stack: Phenomenon and resolution. Renew Energy 2023;219:119392. http://dx.doi.org/10.1016/j.renene.2023.119392.

[52] Schoemaker M, Misz U, Beckhaus P, Beckhaus P, Heinzel A. Evaluation of hydrogen crossover through fuel cell membranes. Fuel Cells 2014;14(3). http://dx.doi.org/10.1002/fuce.201300215.

[53] Tang Q, Li B, Yang D, Ming P, Zhang C, Wang Y. Review of hydrogen crossover through the polymer electrolyte membrane. Int J Hydrog Energy 2021;46(42):22040–61. http://dx.doi.org/10.1016/j.ijhydene.2021.04.050.

[54] Ding F, Zou T, Wei T, Chen L, Qin X, Shao Z, Yang J. The pinhole effect on proton exchange membrane fuel cell (PEMFC) current density distribution and temperature distribution. Appl Energy 2023;342:121136. http://dx.doi.org/10.1016/j.apenergy.2023.121136.

[55] Corbo P, Migliardini F, Veneri O. Experimental analysis of a 20kWe PEM fuel cell system in dynamic conditions representative of automotive applications. Energy Convers Manage 2008;49(10):2688–97. http://dx.doi.org/10.1016/j.enconman.2008.04.001.

[56] Barbir F. CHAPTER 5 - Fuel cell operating conditions. In: Barbir F, editor. PEM fuel cells. Burlington: Academic Press; 2005, p. 115–45. http://dx.doi.org/10.1016/B978-012078142-3/50006-9.

[57] Ayubirad M, Qiu Z, Wang H, Weinkauf C, Ossareh HR. Simultaneous constraint management of hydration and oxygen excess ratio for PEM fuel cells: A parallel cascaded reference governor approach. Energy Convers Manage 2023;295:117629. http://dx.doi.org/10.1016/j.enconman.2023.117629.

[58] Liu Z, Zhang B, Xu S. Research on air mass flow-pressure combined control and dynamic performance of fuel cell system for vehicles application. Appl Energy 2022;309:118446. http://dx.doi.org/10.1016/j.apenergy.2021.118446.

[59] Zhou Y, Chen B, Meng K, Zhou H, Chen W, Zhang N, Deng Q, Yang G, Tu Z. Optimal design of a cathode flow field for performance enhancement of PEM fuel cell. Appl Energy 2023;343:121226. http://dx.doi.org/10.1016/j.apenergy.2023.121226.

[60] Di Ilio G, Di Giorgio P, Tribioli L, Bella G, Jannelli E. Preliminary design of a fuel cell/battery hybrid powertrain for a heavy-duty yard truck for port logistics. Energy Convers Manage 2021;243:114423. http://dx.doi.org/10.1016/j.enconman.2021.114423.

[61] Yin C, Yang H, Liu Y, Wen X, Xie G, Wang R, Tang H. Numerical and experimental investigations on internal humidifying designs for proton exchange membrane fuel cell stack. Appl Energy 2023;348:121543. http://dx.doi.org/10.1016/j.apenergy.2023.121543.